

Original Article

Effect of transverse isotropy on compressive strengths and elastic properties of bedded gypsum

Laksikar Sitthimongkhon, Thanittha Thongprapha, Kiattisak Artkhonghan, and Kittitep Fuenkajorn*

*Geomechanics Research Unit, Institute of Engineering,
Suranaree University of Technology, Mueang, Nakhon Ratchasima, 30000 Thailand*

Received: 20 September 2021; Revised: 11 January 2022; Accepted: 20 January 2022

Abstract

Compression tests have been performed on cylindrical specimens of bedded gypsum under confining pressures up to 15 MPa. The specimens contain different bedding plane orientations. Results indicate that transverse isotropic effect occurs under all confinements where the strength is lowest when the normal to bedding planes makes an angle (β) of 60° with the core axis. The lowest modulus is obtained at $\beta = 0^\circ$, and the highest is at $\beta = 90^\circ$. Confining pressures rapidly increase the elastic and shear moduli normal to bedding plane strike, toward those parallel to the beds. Loading gypsum under high confinement may induce plastic deformation by dislocation climb mechanism, which gradually tightens the microcracks and pore spaces along bedding planes. Coulomb criterion is capable of describing the rock compressive strengths where the cohesion is defined as a polynomial function of β . Distortional strain energy induced at failure coincides with the results obtained from Coulomb criterion.

Keywords: confining pressure, bedding plane, Coulomb criterion, strain energy

1. Introduction

Gypsum deposit in Nakhon Sawan Province, central part of Thailand was rehydrated from the underlain anhydrite. The deposit is in a graben extending over 10 km long in north-south direction. The rock is grey to light grey massive microcrystalline (Kuroda *et al.*, 2017). The volume increase during rehydration under burial condition makes its lamination deformed, undulated and highly distorted (Warren, 1999). Several open pit mines have been operated along the trend of the deposit. In many locations, the slope toes intersect gypsum ore with bedding plane inclinations as high as 45 degrees. Due to the fact that gypsum is a relatively soft rock and exhibits transverse isotropic characteristics, concerns are raised as to the short- and long-term stability of the mine slopes during excavation and after decommissioning.

The anisotropic degree of rocks has been defined as the maximum-to-minimum elastic modulus ratio, or the maximum-to-minimum strength ratio. These properties are

from different directions with respect to the transverse isotropic planes (e.g., bedding planes for sedimentary rocks, foliation planes for metamorphic rocks, or system of microcracks and fractures in rock mass) (Goodman, 1989). Ramamurthy (1993) classifies the rock anisotropy into six types based on the shapes of strength ratio curve versus the transverse isotropic plane angle. These include inherent, induced, cleavage, U-shaped, undulatory and bedding plane anisotropies (Gholami & Rasouli, 2014). Several investigators have found that the degree of anisotropy of rocks decreases with increasing confining pressures. Nasser, Rao, and Ramamurthy (2002) perform compression tests on four Himalayan schists with confining pressures up to 100 MPa, and find that the degree of rock anisotropy in terms of strengths and elastic moduli decreases as the confining pressures increase. The degrees of anisotropy of mudstones compressive strength and static and dynamic elastic moduli obtained by Miller, Plumb, and Boitnott (2013) also decrease as the confining pressures increase. This agrees with the experimental results obtained by Xu, He, Su, and Chen (2018) on phyllite, and by Fereidooni, Khanlari, Heidari, Sepahi, and Kolahi-Azar (2016) on phyllite, slate, hornfels and schist. Test

*Corresponding author

Email address: kittitep@sut.ac.th

results by Hu *et al.* (2017) however suggest that increasing the confining pressures up to 30 MPa does not seem to reduce the degree of anisotropy of interbedded sandstone from Shandong area, China.

The transverse isotropic response has also been observed in time-dependent rocks, such as salt. Rock salt exhibits transverse isotropic structures primarily due to the layers of crystallization and the inclusions (e.g., anhydrite, potash, gypsum, and clay minerals) (Warren, 1999). These inclusions may be interbedded with the salt or disseminate between halite crystals. Jeremic (1994) reports that rock salt from Poland shows the transverse isotropic effect on its uniaxial compressive strength where the minimum strength is obtained when the bedding inclination makes an angle of 45° with the loading direction. Dubey and Gairola (2008) performed uniaxial creep tests on prismatic salt specimens from India under three different bedding orientations (0°, 45° and 90°). Their results indicate that the steady-state creep rate is highest when the bedding planes make an angle of 45° with the loading axis. The lowest rate is observed in the direction normal to the bedding planes. The transverse isotropic effect on salt also tends to decrease with increasing loading rates (Dubey, 2018).

Some knowledge gaps remain. A strength criterion for rocks including gypsum, that exhibit transverse isotropic behavior has never been developed for practical use. The mechanisms controlling the strength and elastic responses of soft rocks under varied confinements have not been identified. These knowledge are needed for the analysis and design of relevant geological structures to ensure their long-term stability.

The objective of this study is to determine the strength and elastic properties of transverse isotropic gypsum. The main tasks involve performing compression tests under confining pressures up to 15 MPa, determining elastic properties for various bedding plane orientations, developing strength criterion that can incorporate the transverse isotropic effect, and applying strain energy principle to predict the strength and deformability of the rock.

. Also, many species of Basidiomycota were isolated from Salahadin and Baghdad Governorates (Al-Khesraji & Suliaman, 2019; Al-Khesraji, Suliaman, Al Hayawi, & Sadiq, 2019).

2. Gypsum Specimens

Gypsum blocks with approximate size of 50×50×50 cm³ have been collected from an open pit mine of Siam Cement Group, Co. in Nakhon Sawan Province. They are cored and cut to obtain cylindrical specimens with nominal diameters of 54 mm and length-to-diameter ratio of 2.0. The nominal angles (β) between the specimen main axis and the normal to bedding planes are selected as 0, 30, 45, 60 and 90 degrees. Results from X-ray diffraction analysis indicate that the specimens contain 88.90% gypsum, 7.98% calcite, 3.0% chlorite and 0.12% anhydrite by weight. Based on petrographic analysis, their crystal sizes range from 0.1 to 0.4 mm. The bedding planes can be observed by alternations of white gypsum and grey anhydrite bands. Their average density determined based on ASTM D6473-15 (2021) is 2.25±0.06 g/cc. The rock porosity is 4.47%. It is determined in accordance with ASTM C97/C97M-18 (2021).

3. Test Apparatus and Method

Test procedure and calculation for the compression test follow the ASTM D7012-14e1 (2021) standard practice. The constant confining pressures are applied by Hoek triaxial cell. A pair of strain gages is installed at the mid-section of the specimen to monitor the circumferential strains parallel and normal to the strike of bedding planes. The axial deformation is measured using displacement dial gages. Gypsum specimens are tested under constant confining pressures (σ_3) of 0, 3, 5, 7, 12, and 15 MPa. The specimen is first subjected to a desired uniform confining pressure. A hydraulic load cell with electric pump increases the axial stress under constant rates of 0.1 MPa/s until failure occurs. The specimen deformations monitored along the three principal directions are used to calculate the principal strains during loading. They are recorded to the nearest 0.001 mm.

4. Test Results

Examples of stress-strain curves and representative images of gypsum specimens prior to testing are given in Figure 1. The diagrams show that the specimens with $\beta = 90^\circ$ (beds are parallel to σ_1) show the lateral strains normal to the strike of bedding planes (ϵ_{30}) notably larger than those parallel to the bedding planes (ϵ_{3P}). The two lateral strains are comparable for specimens with $\beta = 0^\circ$. The specimens with $\beta = 60^\circ$ give the lowest compressive strengths. The highest strengths are obtained from those with $\beta = 0^\circ$. This holds true for all confining pressures. The strength discrepancies between the three angles become smaller, as the confining pressure increases. Table 1 gives the compressive strengths ($\sigma_{1,t}$) for all specimens.

Confining pressure appears to be the predominant factor controlling the modes of failure. Under low confining pressures (7 MPa or less), combination of shear and extensile failures is found for the specimens with $\beta = 0^\circ, 30^\circ$ and 90° . Most specimens with $\beta = 45^\circ$ and 60° show shear failure along their bedding planes. Under σ_3 equal to 12 and 15 MPa, small multiple shear fractures are observed for all bedding plane orientations.

5. Elastic Properties

Assuming that the specimens are linearly elastic, the elastic moduli along the major principal (axial) direction (E_1) and along the two minor principal (lateral) axes normal and parallel to bedding plane strike (E_{30} and E_{3P}) can be calculated from the test results. For the transverse isotropic material (Figure 1d), the strains under triaxial compression can be presented in terms of the applied stresses and elastic parameters as (Jaeger, Cook, & Zimmerman, 2007):

$$\epsilon_1 = \sigma_1/E_1 - \nu_{1,3P} \sigma_3/E_{3P} - \nu_{1,30} \sigma_3/E_{30} \quad (1)$$

$$\epsilon_{3P} = -\nu_{1,3P} \sigma_1/E_1 + \sigma_3/E_{3P} - \nu_{3P,30} \sigma_3/E_{30} \quad (2)$$

$$\epsilon_{30} = -\nu_{1,30} \sigma_1/E_1 - \nu_{3P,30} \sigma_3/E_{3P} + \sigma_3/E_{30} \quad (3)$$

where σ_1 and σ_3 are the major and minor principal stresses, ϵ_1 is the major principal strain, and ϵ_{3P} and ϵ_{30} are the strains

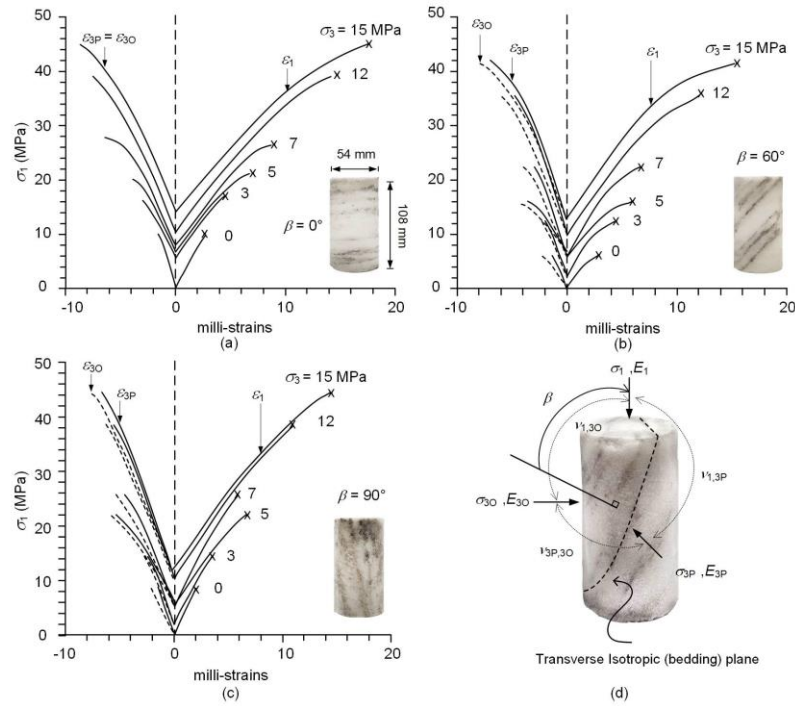


Figure 1. Examples of stress-strain curves on gypsum specimens with $\beta = 0^\circ$ (a), 60° (b), and 90° (c). Notations used in Table 1 (d).

Table 1. Compression test results

β	σ_3 (MPa)	$\sigma_{1,f}$ (MPa)	E_1 (GPa)	E_{3P} (GPa)	E_{30} (GPa)	$\nu_{1,3P}$	$\nu_{1,30}$	$\nu_{3P,30}$
0°	0	9.86	3.34	-	-	0.27	0.27	-
	3	16.90	4.00	8.06	8.06	0.26	0.26	0.21
	5	21.13	4.85	8.11	8.11	0.26	0.26	0.20
	7	26.51	5.54	8.28	8.28	0.25	0.25	0.20
	12	39.14	6.69	8.46	8.46	0.24	0.24	0.20
	15	44.89	7.85	8.93	8.93	0.22	0.22	0.20
30°	0	7.89	3.79	-	-	0.26	0.30	-
	3	13.71	4.48	8.04	6.07	0.25	0.29	0.23
	5	20.10	5.33	8.12	6.74	0.24	0.27	0.23
	7	24.68	6.01	8.29	7.24	0.25	0.26	0.22
	12	37.48	7.10	8.47	7.89	0.23	0.24	0.21
	15	42.96	8.22	8.93	8.73	0.22	0.22	0.21
45°	0	6.71	4.49	-	-	0.25	0.32	-
	3	12.78	5.34	8.03	5.07	0.24	0.29	0.24
	5	17.79	5.94	8.10	5.89	0.23	0.28	0.23
	7	23.39	6.67	8.28	6.51	0.24	0.27	0.23
	12	35.86	7.31	8.46	7.42	0.22	0.25	0.30
	15	42.09	8.31	8.93	8.54	0.21	0.23	0.20
60°	0	5.84	6.32	-	-	0.24	0.31	-
	3	12.12	6.66	8.05	4.44	0.23	0.29	0.26
	5	15.98	7.03	8.08	5.29	0.22	0.28	0.25
	7	22.10	7.27	8.28	5.97	0.22	0.27	0.23
	12	35.00	7.72	8.45	7.03	0.22	0.24	0.23
	15	41.11	8.51	8.96	8.36	0.20	2.22	0.23
90°	0	8.51	8.02	-	-	0.20	0.27	-
	3	14.28	8.06	8.06	4.00	0.21	0.26	0.21
	5	22.04	8.11	8.11	4.85	0.20	0.25	0.20
	7	25.48	8.28	8.28	5.54	0.20	0.25	0.20
	12	38.16	8.46	8.46	6.69	0.20	0.24	0.20
	15	43.81	8.93	8.93	7.85	0.20	0.22	0.20

measured parallel and normal to the strike of bedding planes. For transverse isotropic condition, three Poisson's ratios are defined on the specimens: $\nu_{1,3P}$ and $\nu_{1,3O}$ represent the Poisson's ratios on the planes between the major principal axis and the directions that are parallel and normal to the strike of bedding planes. The $\nu_{3P,3O}$ represents Poisson's ratio between the directions that are parallel and normal to the bedding plane strike.

For $\beta = 0^\circ$ and 90° , the elastic moduli and Poisson's ratios under unconfined condition can be readily calculated from equation (1) to (3). Regression analysis using SPSS code (Wendai, 2000) are performed to determine the elastic parameters of the specimens with $0^\circ < \beta < 90^\circ$. The regression uses the stresses and their corresponding strains obtained from linear portion of the curves from start loading to 40-50% of the failure stress for each specimen. Table 1 gives the results. Under low confining pressures, the intrinsic elastic moduli parallel to bedding plane strike (E_{3P}) are greater than those normal to the strike (E_{3O}) which can be clearly observed for $\beta = 90^\circ$. The stiffness discrepancies decrease with angle β . The two moduli are equal for $\beta = 0^\circ$ (σ_1 is normal to bedding planes). Under high confinement, the elastic moduli for all angles are comparable.

Similar behavior is observed for the Poisson's ratios. Under low confining pressures, the Poisson's ratios parallel to bedding plane strike ($\nu_{1,3P}$) are slightly lower than those normal to the bedding plane strike ($\nu_{1,3O}$). For $\beta = 0^\circ$, the two Poisson's ratios are equal while $\nu_{3P,3O}$ is lower than the two. Under high confinement, the Poisson's ratios measured from all planes are comparable.

6. Amadei's Solutions

The apparent elastic parameters calculated for $0^\circ < \beta < 90^\circ$ are compared with those predicted by Amadei (1996) solutions. He proposes sets of equations to determine the elastic moduli and Poisson's ratios under varied orientations of transverse isotropic planes, providing that the intrinsic elastic parameters for β equal to 0° and 90° are known. Exhaustive review and detailed deviation of Amadei's solutions have been described elsewhere (Amadei, 1996; Gholami & Rasouli, 2014; Miller *et al.*, 2013; Nasser *et al.*, 2002; Nejati, Dambly, & Saar, 2019). They are not repeated here. Based on the generalized Hook's law, for transverse isotropic material, Amadei introduces three variables:

$$E_y = 1/a_{22} \quad (4)$$

$$\nu_{yx} = a_{12}/a_{22} \quad (5)$$

$$\nu_{yz} = a_{23}/a_{22} \quad (6)$$

where E_y is apparent Young's modulus, ν_{yx} and ν_{yz} are apparent Poisson's ratios in x-y-z coordinate system, a_{12} , a_{22} and a_{23} are compliance components. These components are defined as a function of transverse isotropic plane angle (β) as:

$$a_{22} = \cos^4 \beta / E' + \sin^4 \beta / E + \sin^2 2\beta / 4 (1/G' - 2\nu'/E') \quad (7)$$

$$a_{12} = (\nu'/E') \sin \beta - (\nu'/E') \cos^4 \beta + (\sin^2 2\beta / 4) (1/E + 1/E' - 1/G') \quad (8)$$

$$a_{23} = (\nu'/E') \cos 2\beta - (\nu/E) \sin^2 \beta \quad (9)$$

where E and E' are intrinsic Young's moduli parallel and normal to strike of transverse isotropic plane, ν and G are Poisson's ratio and shear modulus on transverse isotropic plane, ν' and G' are Poisson's ratio and shear modulus on the plane normal to transverse isotropic plane. These parameters interrelate as follows:

$$1/G' = 1/E + 1/E' + 2\nu'/E' \quad (10)$$

$$1/G = 2(1+\nu)/E \quad (11)$$

Note that the intrinsic moduli E and E' are equivalent to E_1 values for $\beta = 90^\circ$ and 0° , and ν and ν' are equivalent to $\nu_{1,3P}$ and $\nu_{1,3O}$ for $\beta = 90^\circ$ defined from our testing (Table 1). Substituting these parameters into equation (7) to (9) and subsequently into equation (4) to (6), the apparent Young's moduli and Poisson's ratios under all confining pressures and bedding plane angles can be determined.

Polar plot provided in Figure 2 gives example of the apparent Young's moduli comparing with the test results for different confining pressures. The Young's moduli for all bedding plane angles become similar as the confining pressure increases to 15 MPa. This agrees with the Amadei's prediction (lines in Figure 2). The apparent Poisson's ratios on y-x plane (ν_{yx}) and y-z plane (ν_{yz}) slightly depend on the bedding plane orientations (β), as indicated by lines and data points in Figure 3. Their transverse isotropic responses tend to reduce as the confining pressure increases toward 15 MPa.

The similarity and discrepancy between the test results and the Amadei's predictions can be evaluated using the mean misfit (s) as an indicator. It is calculated by (Riley, Hobson, & Bence, 1998):

$$s = 1/m (\sum_i^m s_i) \text{ where } s_i = [(1/n) (\sum_{j=1}^n (X_{j,p} - X_{j,t})^2)]^{1/2} \quad (12)$$

where $X_{j,p}$ and $X_{j,t}$ are the predicted and measured Young's moduli or Poisson's ratios, n is the number of bedding plane angles (β) used for each confining pressure, and m is the number of confining pressure. The maximum mean misfit for the Young's moduli is calculated as 0.14 MPa, and for Poisson's ratios are 0.01 (for ν_{yz}) and 0.01 (for ν_{yx}). These low misfit values indicate good agreements between the measured elastic parameters and the Amadei's predictions.

7. Degree of Anisotropy

Figure 4 plots the degree of anisotropy of gypsum in the form of the maximum-to-minimum elastic modulus ratios (E_{90}/E_0) as a function of confining pressure, where E_{90} and E_0 are measured parallel and normal to the bedding plane. The degrees of modulus anisotropy of various rocks obtained elsewhere are also compared in the figure. Gypsum tends to show lower degree of anisotropy, and reduces toward the isotropic condition much quicker, as compared to other more brittle and stronger rocks. It, however, shows a higher degree

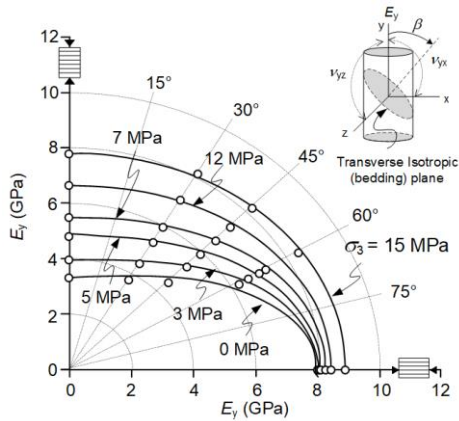


Figure 2. Polar plot of apparent elastic moduli (E_β) under different bedding plane angles (β). Points are test results, lines are Amadei's predictions.

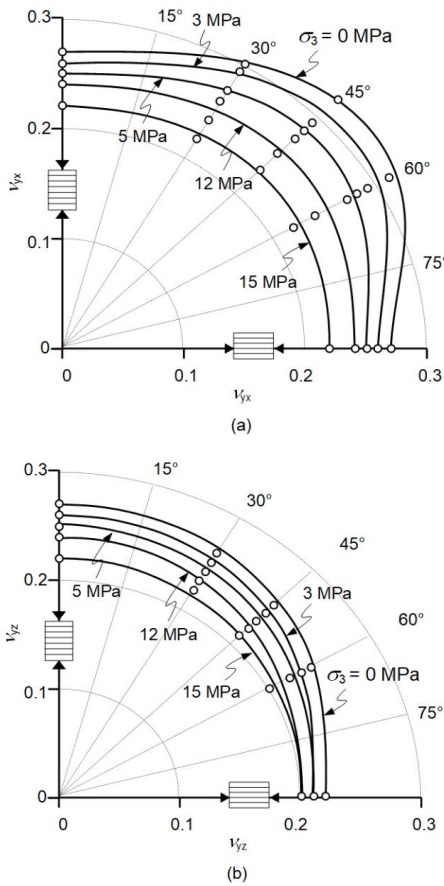


Figure 3. Polar plot of apparent Poisson's ratios ν_{yx} (a) and ν_{yz} (b). Points are test results, lines are Amadei's predictions.

of anisotropy than rock salt obtained by Hatzor and Heyman (1997).

To reveal how the degree of anisotropy for gypsum reduces as the confining pressure increases, the elastic moduli obtained along the major principal (axial) direction for different angles β are plotted as a function of confining pressure in Figure 5. They are designated as E_β , where β are

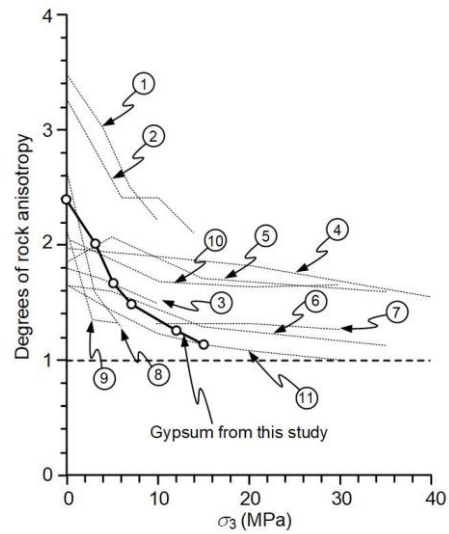


Figure 4. Degrees of rock anisotropy (E_{90}/E_0) as a function of confining pressure. ① Hornfels, ② Schist, ③ Garnet hornfels (Fereidooni *et al.*, 2016); ④ Mudstone (Miller *et al.*, 2013); ⑤ Quartzitic schist, ⑥ Biotite schists (Nasseri *et al.*, 2003); ⑦ Phyllite (Xu *et al.*, 2018); ⑧ Meta-siltstone, ⑨ Schist (Usoltseva *et al.*, 2017); ⑩ Sandstone (Hu *et al.*, 2017); ⑪ Rock salt (Hatzor and Heyman, 1997)

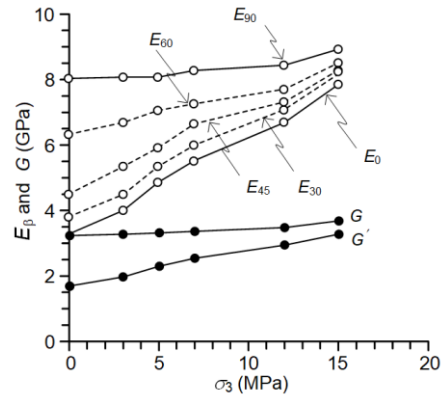


Figure 5. Intrinsic and apparent elastic and shear moduli increase with confining pressure (σ_3). Intrinsic elastic parameters parallel to beds (E_{90} , G) always greater than those normal to beds (E_0 , G'). Apparent elastic moduli (for $0 < \beta < 90^\circ$) are between the two intrinsic values.

0° , 30° , 45° , 60° and 90° . The shear moduli on the bedding planes (G) and on the plane perpendicular to the beds (G'), are also given. These shear moduli are calculated from equations (10) and (11).

Under unconfined condition, E_{90} is the highest, obtained when σ_1 is parallel to the bedding planes. They slightly increase with confining pressure. The lowest elastic moduli are E_0 obtained when the bedding planes are perpendicular to σ_1 . These elastic moduli increase, as the beds dip away from the major principal axis, as shown by E_{30} , E_{45} and E_{60} . They also increase rapidly toward E_{90} as the confining pressures increase. The increase of these moduli is presumably due to the closure of micro-cracks and inter-

crystalline boundaries parallel to the bedding planes, and the stiffening of the soft layers by the confinement. Such behavior is supported by the apparent elastic moduli diagram shown in Figure 2. Similar behavior is observed from the shear moduli. The confining pressures slightly increase G , but considerably increase G' . These processes decrease the degree of anisotropy of the gypsum as the confining pressure increases.

8. Strength Criterion

An attempt is made here to incorporate the transverse isotropic effects into the Coulomb criterion. The major principal stress at failure ($\sigma_{1,f}$) can be expressed as a function of confining pressure (σ_3) as (Jaeger *et al.* 2007):

$$\sigma_{1,f} = \frac{[(1 + \sin \phi)/(1 - \sin \phi)] \cdot \sigma_3 + (2c \cdot \cos \phi)}{(1 - \sin \phi)} \tag{13}$$

where c and ϕ are cohesion and internal friction angle. Figure 6 plots the Coulomb criterion for all bedding plane angles, β . The multiplier of σ_3 represents slope of the curves and the last term on the right side of equation (13) is the intercept on $\sigma_{1,f}$ axis. The cohesion and friction angle can be determined by regression analysis of the strength data. It is found that the friction angles tend to be independent of the bedding plane orientation (β), where their average value is 24 degrees. The cohesions, however, vary with the bedding plane orientation. Their numerical values are given in Figure 6. The lowest cohesions are obtained from the specimens with $\beta = 60^\circ$, and the highest ones are from those with $\beta = 0^\circ$. A third-degree polynomial equation can best describe the relationship between the cohesions and angle β as:

$$c = c_0 + A \cdot \beta + B \cdot \beta^2 + C \cdot \beta^3 \tag{14}$$

where c_0 is the cohesion obtained from specimens with $\beta = 0^\circ$, and A , B and C are empirical constants. Their numerical values obtained from regression analysis are given in Figure 7. Good correlation is obtained ($R^2 > 0.990$).

9. Strain Energy Density Criterion

In order to consider both stresses and strains, the strain energy principle is applied to describe the gypsum failure under different bedding orientations. Distortional strain energy (W_d) and mean strain energy (W_m) at failure are calculated for each specimen using the following equations (Jaeger *et al.* 2007):

$$W_d = (3/2) \cdot \tau_{oct, f} \cdot \gamma_{oct, f} \tag{15}$$

$$W_m = (3/2) \cdot \sigma_{m, f} \cdot \varepsilon_{m, f} \tag{16}$$

where $\tau_{oct, f}$ and $\gamma_{oct, f}$ are octahedral shear stress and strain at failure, and $\sigma_{m, f}$ and $\varepsilon_{m, f}$ are mean stress and mean strain. They are calculated by:

$$\sigma_{m, f} = (\sigma_{1, f} + 2\sigma_3)/3 \tag{17}$$

$$\varepsilon_{m, f} = (\varepsilon_{1, f} + \varepsilon_{3P, f} + \varepsilon_{3O, f})/3 \tag{18}$$

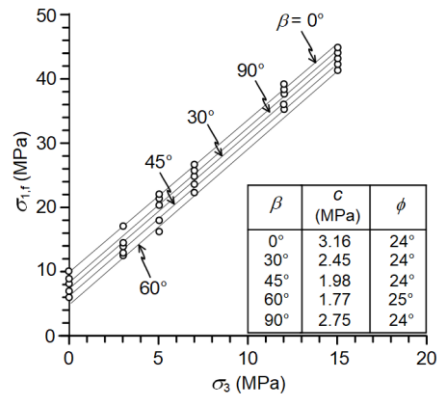


Figure 6. Major principal stresses at failure ($\sigma_{1,f}$) as a function of confining pressure (σ_3). Lines are Coulomb criterion.

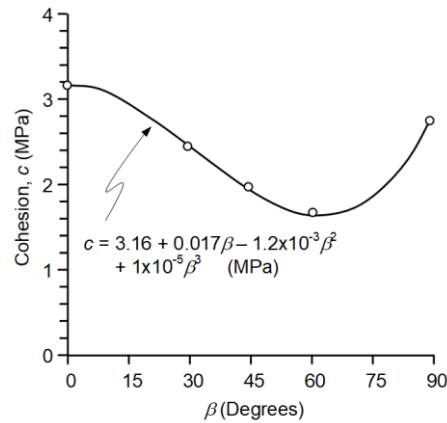


Figure 7. Cohesions as a function of bedding plane orientation

where $\varepsilon_{1,f}$, $\varepsilon_{3P,f}$ and $\varepsilon_{3O,f}$ are principal strains at failure. Linear equation is proposed to represent W_d as a function of W_m :

$$W_d = \delta \cdot W_m + \alpha \tag{19}$$

where δ represents slope of W_d - W_m relations, and α is W_d for $W_m = 0$. Figure 8 compares the calculated W_d and W_m with the proposed equations for all angles β . Correlation coefficients (R^2) are greater than 0.990. Numerical values for δ and α are given in the figure. The diagram indicates that the W_d - W_m relation obtained at $\beta = 60^\circ$ shows the lowest value but gives the steepest slope ($\delta = 1.611$). As a result, the higher W_d - W_m relations for $\beta = 45^\circ, 30^\circ, 90^\circ$ and 0° would terminate on the 60° W_d - W_m relation at $W_m = 0.063, 0.064, 0.079$ and 0.088 MPa, respectively. It seems that, W_d for $\beta = 60^\circ$ continues to increase linearly with W_m beyond these termination points, suggesting that it would be able to describe the gypsum strength from transverse isotropic to isotropic behavior.

The strain energy relations implicitly incorporate both stresses and strains, and hence they may be more suitable for use as a failure criterion for the gypsum. This is primarily because gypsum deformability is significant under failure, as compared to other hard and brittle rocks. The W_d - W_m failure criterion agrees well with those of the Coulomb criterion proposed earlier. Both suggest that gypsum failure and

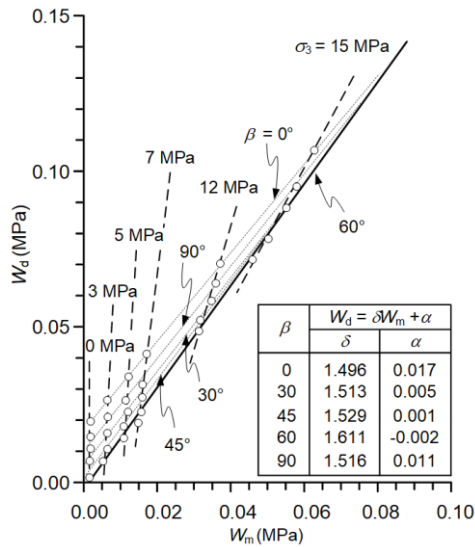


Figure 8. Distortional strain energy (W_d) at failure as a function of mean strain energy (W_m)

deformability obtained for $\beta = 60^\circ$, where it exhibits the lowest strength, can be extended to the condition where it mechanically responds as isotropic material under higher confinement beyond the range tested here.

10. Discussions and Conclusions

The confining pressure significantly reduces the transverse isotropic responses of the gypsum in the forms of elastic moduli. Increasing the confining pressures presumably reduce the porosity, stiffen the soft layers, and tighten the micro-cracks and along the bedding planes. This agrees with results obtained by Lyu *et al.* (2021) who experimentally show that increasing confining pressures can effectively reduce microcracks, pore spaces and permeability of gypsum specimens obtained from China. Under subsequent differential stress application, deformability of the micro-crystalline gypsum is likely governed by dislocation climb mechanism (time-dependent sliding between inter-crystalline boundaries). This process reduces the transverse isotropic response of the rock, as the applied load cannot well recognize the transverse isotropic (bedding) planes. As the differential stress progressively increases toward failure, only small shear fractures are initiated and propagated along the tight inter-crystalline boundaries.

Specimens with $\beta = 60^\circ$ allow shear fractures to propagate more easily along the inter-crystalline boundaries of the bedding planes, leading to the lowest compressive strengths. These processes would be similar to those of other transverse isotropic rocks, as addressed by several investigators, e.g. Dubey and Gairola (2008), Fereidooni *et al.* (2016) and Nessei *et al.* (2002).

It is recognized that there are two main mechanisms governing the non-linear or plastic behavior of soft crystalline rocks (e.g. rock salt, potash and gypsum): dislocation climb and dislocation glide (sliding between cleavage planes) (Fuenkajorn & Daemen, 1988; Fuenkajorn, Sriapai, & Samsri, 2012). Only dislocation climb is induced in the gypsum tested here because it is a fine grained (0.1-0.4 mm) rock, has

relatively high porosity (4.47%), and is compressed for relatively short duration. Sliding between the cleavage planes is likely induced in those with large crystals under long-term loading and large confinements, as experimentally evidenced by Langer (1984).

The mechanism governing the reduction of the degree of gypsum anisotropy described above may not be true for other strong and brittle rocks. The mechanisms controlling their deformability are likely different, depending on rock types and their transverse isotropic characteristics, as described by Ramamuthy (1993) and Gholami and Rasouli (2014). Unlike gypsum, strong and brittle rocks may not be that sensitive to the confining pressure in terms of their strength and deformability.

It is recognized that there are other factors influencing the transverse isotropic responses of the rocks, which are excluded from this study. These include, for example, moisture content, specimen size, and wet-dry cycles. These factors may be encountered under in-situ conditions which may alter the results obtained here. For example, pore pressure may reduce compressive strengths and elastic moduli of the rock, as experimentally evidenced by Khamrat, Archeeploha, and Fuenkajorn (2016). Further studies on these effects are desirable.

The approach presented in this study may be transferable to other soft and transverse isotropic rocks. The angles of their transverse isotropic planes corresponding to the lowest strength and stiffness, however, may be different from the gypsum tested here.

Conclusions drawn from this study can be summarized as follows.

- Within the range of confinements used here, gypsum specimens give the highest elastic moduli when the normal to bedding planes makes an angle (β) of 90° with the major principal axis, the lowest values are obtained when $\beta = 0^\circ$ (beds are normal to σ_1). The elastic modulus and Poisson's ratios measured for $0^\circ < \beta < 90^\circ$ agree reasonably well with those predicted by Amadei's solutions. The gypsum compressive strengths are highest at $\beta = 0^\circ$, and lowest at $\beta = 60^\circ$.
- The confining pressures reduces the degree of rock anisotropy by stiffening the soft layers and closing the micro-cracks along the bedding planes. The confinement rapidly increases the elastic and shear moduli normal to bedding plane strike and approaches those parallel to the bedding planes.
- Coulomb criterion implicitly incorporates the transverse isotropic effect by defining the cohesion as a polynomial function of bedding plane angles. It agrees well with the test results.
- The strain energy criterion reveals that the maximum distortional strain energy densities that the gypsum can sustain before failure, depend on the bedding plane orientation. The W_d - W_m relations for $\beta = 60^\circ$ give the lowest energies while the highest ones are from $\beta = 0^\circ$. This agrees with the strength results obtained from the Coulomb criterion.

Acknowledgements

This work was supported by Suranaree University of Technology (SUT) and Thailand Science Research and Innovation (TSRI). Permission to publish this paper is gratefully acknowledged.

References

- Amadei, B. (1996). Importance of anisotropy when estimating and measuring in situ stresses in rock. *International Journal of Rock Mechanics and Mining Sciences and Geomechanics Abstracts*, 33(3), 293-325.
- American Society for Testing and Material C97 / C97M-18. (2021). Standard test methods for absorption and bulk specific gravity of dimension stone. *Annual Book of ASTM Standards*. West Conshohocken, PA: Author.
- American Society for Testing and Material D6473-15. (2021). Standard test method for specific gravity and absorption of rock for erosion control. *Annual Book of ASTM Standards*. West Conshohocken, PA: Author.
- American Society for Testing and Material D7012-14e1. (2021). Standard test methods for compressive strength and elastic moduli of intact rock core specimens under varying states of stress and temperatures. *Annual Book of ASTM Standards*. West Conshohocken, PA: Author.
- Dubey, R. (2018). Bearing of structural anisotropy on deformation and mechanical response of rocks: An experimental example of rocksalt deformation under variable compression rates. *Journal of the Geological Society of India*, 91(1), 109-114.
- Dubey, R. K., & Gairola, V. K. (2008). Influence of structural anisotropy on creep of rocksalt from Simla Himalaya, India: An experimental approach. *Journal of Structural Geology*, 30(6), 710-718.
- Fereidooni, D., Khanlari, G., Heidari, M., Sepahi, A. A., & Kolahi-Azar, A. P. (2016). Assessment of inherent anisotropy and confining pressure influences on mechanical behavior of anisotropic foliated rocks under triaxial compression. *Rock Mechanics and Rock Engineering*, 49, 2155-2163.
- Fuenkajorn, K., & Daemen, J. J. K. (1988). *Borehole closure in salt*. Technical report (NU REG/CR-5243 RW) prepared for the office of Nuclear Regulatory Research, U.S. Nuclear Regulatory Commission, Washington D.C. 20555. Tucson, AZ: University of Arizona.
- Fuenkajorn, K., Sriapai, T., & Samsri, P. (2012). Effects of loading rate on strength and deformability of Maha Sarakham salt. *Engineering Geology*, 135-136, 10-23.
- Gholami, R., & Rasouli, V., (2014). Mechanical and elastic properties of transversely isotropic slate. *Rock Mechanics and Rock Engineering*, 47(5), 1763-1773.
- Goodman, R. E., (1989). *Introduction to rock mechanics* (2nd ed.). New York, NY: Wiley.
- Hatzor, Y. H., & Heyman, E. P. (1997). Dilation of anisotropic rock salt: Evidence from Mount Sedom diapir. *Journal of Geophysical Research: Solid Earth*, 102(B7), 14853-14868.
- Hu, S., Tan, Y., Zhou, H., Guo, W., Hu, D., Meng, F., & Liu, Z. (2017). Impact of bedding planes on mechanical properties of sandstone. *Rock Mechanics and Rock Engineering*, 50(8), 2243-2251.
- Jaeger, J. C., Cook, N. G. W., & Zimmerman, R. W. (2007). *Fundamentals of Rock Mechanics*. Oxford, England: Blackweel.
- Jeremic, M. K. (1994). *Rock Mechanics in Salt Mining*. Rotterdam, Netherlands: A.A. Balkema.
- Khamrat, S., Archeeploha, S., & Fuenkajorn, K. (2016). Pore pressure effects on strength and elasticity of ornamental stones. *ScienceAsia*, 42, 121-135.
- Kuroda, J., Hara, H., Ueno, K., Charoentitirat, T., Maruoka, T., Miyazaki, T., . . . Lugh, S. (2017). Characterization of sulfate mineral deposits in central Thailand. *Island Arc*, 26(2), e12175.
- Langer, M. (1984). The rheological behaviour of rock salt, mechanical behavior of salt I. *Proceedings of the First Conference on the Mechanical Behavior of Salt*, pp. 201-240. Clausthal-Zellerfeld, Germany: Trans Tech Publications.
- Lyu, C., Liu, J., Wu, Z., Liu, H., Xiao, F., & Zeng, Y. (2021). Experimental study on mechanical properties, permeability and acoustic emission characteristics of gypsum rock under THM coupling. *Rock Mechanics and Rock Engineering*, 54(11), 5761-5779.
- Miller, D., Plumb, R., & Boitnott, G., (2013). Compressive strength and elastic properties of a transversely isotropic calcareous mudstone. *Geophysical Prospecting*, 61(2), 315-328.
- Nasseri, M. H. B., Rao, K. S., & Ramamurthy, T., (2002). Anisotropic strength and deformational behavior of Himalayan schists. *International Journal of Rock Mechanics and Mining Sciences*, 40(1), 3-23.
- Nejati, M., Dambly, M. L. T., & Saar, M. O. (2019). A methodology to determine the elastic properties of anisotropic rocks from a single uniaxial compression test. *Journal of Rock Mechanics and Geotechnical Engineering*, 11(6), 1166-1183.
- Ramamurthy, T. (1993). *Strength and modulus responses of anisotropic rocks*. Oxford, England: Pergamon.
- Riley, K. F., Hobson, M. P., & Bence, S. J. (1998). *Mathematical methods for physics and engineering*. Cambridge, England: Cambridge University Press.
- Usoltseva, O. M., Tsoi, P., & Semenov, V. N. (2017). Effects of structure on deformation and strength characteristics of transversely isotropic man-made geomaterials. *IOP Conference Series: Earth and Environmental Science*, 53, 012009.
- Warren, J. K., (1999). *Evaporites: Their evolution and economics*. Oxford, England: Blackwell Science.
- Wendai, L. (2000). *Regression analysis, linear regression and probit regression. SPSS for windows: Statistical analysis*. Beijing, China: Publishing House of Electronics Industry.
- Xu, G., He, C., Su, A., & Chen, Z. (2018). Experimental investigation of the anisotropic mechanical behavior of phyllite under triaxial compression. *International Journal of Rock Mechanics and Mining Sciences*, 104, 100-112.